Heliyon 9 (2023) e12634

Contents lists available at ScienceDirect

Heliyon

journal homepage: www.cell.com/heliyon

Research article

Evaluation of cytotoxicity, loading, and release activity of paclitaxel loaded-porphyrin based metal-organic framework (PCN-600)

Khadijeh Hamidian [a], Mahmood Barani [b], Mahboubeh Adeli-Sardou [c,d], Mina Sarani [e,*], Saba Daliran [f], Ali Raza Oveisi [f,**]

[a] Department of Pharmaceutics, Faculty of Pharmacy, Zabol University of Medical Sciences, Zabol, Iran
[b] Medical Mycology and Bacteriology Research Center, Kerman University of Medical Sciences, 76169-13555, Kerman, Iran
[c] Herbal and Traditional Medicines Research Center, Kerman University of Medical Sciences, Kerman, Iran
[d] Department of Biotechnology, Institute of Science and High Technology and Environmental Sciences, Graduate University of Advanced Technology, Kerman, Iran
[e] Zabol Medicinal Plants Research Center, Zabol University of Medical Sciences, Zabol, Iran
[f] Department of Chemistry, University of Zabol, P.O. Box: 98615-538, Zabol 9861335856, Iran

ARTICLE INFO

Keywords:
PCN-600
Drug delivery
Paclitaxel
Anticancer drugs
Metal-organic frameworks

ABSTRACT

Considering the inducement side impacts and precipitation of continual doses in conventional therapeutic treatments, there is an urgent need in the field of drug delivery for novel designs of biocompatible carriers with wide loading dimensions and particularly the ability to control their drug release. In this work, we succeeded in synthesizing an iron-based organic metal framework based on iron-porphyrin (PCN-600) through a solvothermal method to function as a drug delivery system (DDS). According to SEM results, PCN-600 crystals a hexagonal-rod shaped morphology with the length of 300 nm and width of 100–300 nm. As an anticancer drug, Paclitaxel (PTX) was successfully loaded into the porphyrin-based metal-organic framework (PCN-600) *via* in-situ encapsulation; the loading efficiency was measured to be about 87.3%. In addition, PTX-encapsulated PCN-600 displayed a controlled and sustained release for up to 24 h of release assessment at the physiological microenvironment of pH = 7.4.

1. Introduction

As a complex disease, the threat of cancer towards modern society is still treated by the dominant method of chemotherapy, while the direct injection of drugs is impossible due to certain limitations such as adverse side effects and poor biological classification [1, 2]. For this reason, scientists have made great efforts to find suitable drug carriers with the ability to unfetter the drugs through a controlled posture and help in reducing the side effects while increasing the effectiveness of applied drug [3, 4].

Cancer is caused by the accumulation of body mutations in the cells. Mutated cells have a competitive advantage over the healthy cells of the body [5, 6]. Breast cancer stands as the most prevalent type of cancer in women that implicate the diagnosis of more than a million patients on a yearly basis [7]. During the process of becoming cancerous, malignant cells grow and multiply abnormally while

* Corresponding author.,
** Corresponding author.
E-mail addresses: minasarani64@gmail.com, m.sarani@zbmu.ac.ir (M. Sarani), aroveisi@uoz.ac.ir (A.R. Oveisi).

https://doi.org/10.1016/j.heliyon.2022.e12634
Received 9 August 2022; Received in revised form 22 November 2022; Accepted 19 December 2022
Available online 26 December 2022

invading the surrounding tissues, which leads to occurrence of invasion and metastasis [7, 8]. Metastasis is a major cause of death for cancer patients that is characterized by the transfer of cancer cells to lymph nodes, bone marrow, lungs, and liver. Despite the advancements of cancer treatment, the prognosis of patients with metastasis remains to be weak and unsatisfactory [9].

Paclitaxel is recognized as a customary and practical chemotherapy drug applied throughout the treating process of cancer. Numerous assessments confirmed the high in vitro and in vivo efficacy of this drug. Paclitaxel (PTX) is a regularly prescribed item among the other chemotherapy drugs for various cancers such as ovarian cancer, breast, uterine, and lung cancers. Nevertheless, its clinical exertion is limited by its insufficient solubility in water. Also, the current clinical administration of its adjuvant results in serious side effects, while exhibiting adverse pharmacokinetics and bioavailability [10]. Therefore, the development of alternative drug delivery systems for PTX is a necessity to increase its solubility, permeability, and stability, as well as to promote sustainable, controlled, and targeted delivery that would exceed its therapeutic impacts and reduces the side effects [11, 12].

The goals of developing new drug delivery mechanisms are to facilitate the ability to control the releasing rate of a drug, maintain the drug concentration within the treatment range for an appropriate period of time, and pave the way for performing specified deliveries of a drug to the target tissue [13, 14]. Many studies attempted to focus on increasing the therapeutic efficacy of anticancer drugs throughout tumor-specific drug deliveries [15, 16, 17]. The applicability of traditional chemotherapy can be disturbed in some cases due to the tendency of anticancer drugs to spreading throughout the body and destroying all the cells [16]. In this regard, targeting cancer cells by the usage of loaded nanoparticles with anti-cancer agents can be a promising approach. Nanoparticle-built drug delivery products have the power to provide the better penetration of particles into the body's cells, which is dependent on their size, and facilitating the delivery through intravenous injection, subcutaneous implantation, or other means [18]. The delivery of drugs with small particle sizes allows a faster dissolution in the bloodstream and leads to the performance of selected drug deliveries to a particular cell or tissue [19, 20].

Over the years, scientists have developed and studied many types of nanoparticles for this particular purpose, including liposomes, micelles, dendrimers, ceramic nanoparticles, and metal nanoparticles, each of which implicate advantages and disadvantages [21]. A suitable drug carrier system is required to contain the following characteristics: 1- High loading capacity, 2- Sizes in nanoscale, 3- Biodegradability, and 4- Non-toxicity or minimal toxicity. Metal-organic frameworks (MOFs) gained lots of interest in recent years in many fields of medicine specially in diagnosis and treatment of cancers [22, 23]. MOFs are included among the varying drug carriers used in modern pharmaceutical systems, which are known as the hybrids of porous organic-mineral materials that are consisted of metal moieties and organic linkers with self-aggregating abilities [21, 24, 25]. The pore size of these porous materials is completely dependent on the size and length of linkers. In other words, the application of larger linkers can result in achieving a larger pore size [26]. MOFs are recognized as unique structures among the porous compounds due to their superior properties such as the ability to offer adjustable structures and functionalities, as well as containing biocompatibility (in some cases), high surface area, and stability [26]. Therefore, many types of these materials have been explored for pharmaceutical or biomedical applications. However, the MOFs that contain micropores lead to excluding the maximum drug loading. To solve this problem, researchers attempted to focus on mesoporous MOFs and their applications in pharmacy management systems [27].

PCN-600 (PCN referring to Porous Coordination Network) is a mesoporous MOF composed of porphyrin linker and Fe-node units that can offer a unique chemical stability, unusual porosity, and suitable biocompatibility. The six-connected $Fe_3O(OOC)_6$ bridges the four-connected porphyrinic-Fe(III) linker to form a 3D network. PCN-600(Fe) as a peroxidase mimic displays one-dimensional (1D) channels in the size of 3.1 nm along with the maximum loading of a gas in the pores of 1.80 $cm^3\ g^{-1}$ in the field of porphyrin-based MOFs. Remarkably, it exhibited a high stability throughout the aqueous mixtures of HCl or NaOH in an inclusive pH scale of 2–11 [28, 29]. In addition, porphyrins and metalloporphyrins are also known for their capabilities in magnetic resonance imaging [29]. Furthermore, iron, which functions as the structural node, is one of the most abundant substances on earth. Therefore, this work attempted to study the design of an iron-based organic metal framework based on iron-porphyrin (PCN-600) as a new carrier to evaluate the drug delivery rate of paclitaxel as an anti-cancer drug.

2. Experimental section

2.1. Martials and methods

The exerted iron (III) nitrate nonahydrate, iron (II) chloride tetrahydrate, pyrrole, propionic acid, sodium acetate, and other chemicals were monetarily procured from Sigma-Aldrich or MERCK to be exerted unescorted by any other purifying processes. The Fe-TCPP linker (iron (III) meso-tetra(4-carboxyphenyl) porphine chloride) and porous PCN-600 were synthesized based on the previously reported procedures with some changes that are mentioned in the following.

2.2. Instruments

We conducted the FE-SEM (field emission scanning electron microscope) imaging and EDX (energy dispersive X-ray spectra) examinations by the usage of TESCAN MIRA3, Czech Republic. Additionally, the X-ray diffraction powder was completed through a X'Pert3 Powder diffractometer, CuKa irradiation, while the Fourier transform infrared spectroscopy (FT-IR, 400- 4000 cm^{-1}) was performed by Perkin Elmer's Spectrum 100 FTIR, USA.

2.3. Synthesizing process of $[Fe_3O(OOCCH_3)_6OH].2H_2O$

It was required to liquefy $Fe(NO_3)_3.9H_2O$ (8 g) and $Na(OOCCH_3).3H_2O$ (11 g) in 9 mL of deionized water under stirring conditions up to the point of obtaining a deep-brown precipitation. Subsequent to filtering and cleansing by cold deionized water, the precipitation was dried at 100 °C overnight.

2.4. Synthesizing process of PCN-600

To prepare PCN-600, 80 mg of $[Fe_3O(OOCCH_3)_6OH].2H_2O$, and 5 mL of DMF were poured into a 20 mL glass vial (I). Then, we appended 80 mg of Fe-TCPP and 12 mL of DMF to another vial (II). Solution I was added to solution II to be sonicated and thus, the vial was incubated at 150 °C for 14 h to achieve a purple solid resultant. The resultant material was washed with DMF (3 times) and acetone (2 times) to be soaked in acetone for 24 h in prior to being dried at room temperature (60 °C (1 h) and 120 °C (12 h)).

2.5. Cytotoxic test

2.5.1. Cell culture

Herein, we employed a human breast cancer cells (MCF-7) line for examining the cytotoxic behavior of PCN-600, PTX, and PTX-loaded PCN-600. The provided MCF-7 cells by the Pasteur Institute of Iran were defrosted to proceed through the culturing step, which were put under centrifugation at 833 rpm for 9 min subsequent to being resettles at Falcon tubes. Next to the dispatching of supernatant, we appended an entire culture medium to the cells and poured the arranged suspensions into the flasks. As the cell culturing procedure was completed by the exertion of DMEM culture medium, the microbial extension was prohibited through the usage of 10% fetal bovine serum (FBS), 100 μg/mL of streptomycin, and 100 international units/mL of penicillin in every culture medium. The cells proliferation and growth was facilitated by the incubation of culture medium under 5% CO_2 at the temperature of 37 °C.

2.5.2. MTT assay

The culturing process of human breast cancer (MCF-7) cells required the exertion of high glucose DMEM equipped with 10% fetal bovine serum and 1% penicillin/streptomycin solution within an incubator (37 °C, 5% CO_2) up to the point of reaching 10000 cells count in every well. Then, we restored the culture medium by 100 μL of DMEM, which contained specific formulations at different concentrations (0–640 μg/mL), to be seeded for an extra 24 h. It should be mentioned that three duplications were dedicated to every concentration. We changed and restored the culture medium after 24 h by the usage of fresh high glucose DMEM. Once 20 μL of 5 mg/mL 3-(4, 5-dimethylthiazol-2-yl)-2, 5-diphenyl tetrazolium bromide (MTT) solution was appended to every well, another incubation process was performed for 4 h. In the following, 100 μL of DMSO was appended to every single well and the obtained resultant was put under shaking conditions for around 15 min at ambient temperature to liquefy the formazan. A microplate reader was employed to determine the optical density (OD) at 570 nm, which was followed by calculating the rate of cell viability (VR, $VR = A/A_0 \times 100\%$, in which A refers to the absorbance of treated cells with formulations and A_0 is the absorbance of control group).

2.5.3. IC50

The calculation of IC50 was based on the survival rate and obtained through the results of MTT test, in which the survival percentage of the treatment with any concentration of free drug or nano-formula was placed in Graphpad Prism V.5 software and achieved as μg/mL.

2.6. Loading capacity

1 mL of PTX solution (120 μg/mL) was added to 5 mL of PCN-600 (1.3 mg/mL) of PBS solution. Subsequent to undergoing ultrasonic for 3 min at 25 °C and being stirred for 24 h at ambient temperature, the obtained MOF was washed and centrifuged to separate the unloaded PTX drug from the loaded PCN-600. Finally, the supernatant was collected to determine the loaded PTX content, while UV-Vis spectroscopy was used to detect the PTX concentrations at 230 nm. The presented equation below was applied to configure the value of loading efficiency (Eq. (1)):

$$\%\text{Loading efficiency} = (\text{Total PTX-PTX in supernatant})/\text{Total PTX} \times 100 \quad (1)$$

2.7. Release study

The conduction of drug release was initiated by dispersing 0.01 g of loaded PCN-600 in 50 mL of PBS (pH 7.4) solution at room temperature. At specific time intervals, we isolated 1 mL of the supernatant for measurement purposes and had it restored by a fresh medium in a similar volume. The absorption of released PTX was investigated by the application of UV-Vis measurements at 230 nm and calculated by below equation (Eq. (2)).

$$\%\ \text{Drug release} = \text{Amount of released drug}/\text{Total drug amount} \times 100 \quad (2)$$

Also, the outcomes of in vitro release were fitted to varying mathematical equations for providing a deeper comprehension of drug release kinetics and mechanisms. Several kinetic equations were exerted to mathematically examine the kinetic attitude and releasing system of PTX from MOF. The outcomes of release assessment were fitted with a number of mathematical equations (Eqs. (3), (4), (5), and (6)) similar to zero-order kinetics, first-order kinetics, Higuchi kinetics and Peppas.

$$Qt = Q0 + k0\ t \tag{3}$$

$$Qt = \log\ Q0 + k1.t/\log\ 2.303 \tag{4}$$

$$Qt = kH.t1/2 \tag{5}$$

$$Mt/M = kptn \tag{6}$$

In which Q_t refers to the cumulative percentage of drug released at time t, M_t/M stands as the fraction of drug released, and k_0, k_1, k_H and k_p represent the constants of zero, first, Higuchi, and Peppas model. Q_0 presents the total volume of loaded drug and n denotes the exponent associated with the releasing system, which is described as the diffusional exponent. We configured the foremost-fit model equation and operating technique of drug release by employing the correlation coefficient of (R^2).

3. Result

3.1. PCN-600 preparation and characterization

PCN-600 was synthesized through the solvothermal reaction of $[Fe_3O(OOCCH_3)_6OH].2H_2O$ and the ligand Fe-TCPP at 150 °C for 14 h (Schemes 1A and 1B, presents the experimental section in details).

As presented in Figures 1A and 1B, the SEM results revealed the hexagonal-rod shaped morphology of PCN-600 crystals (length: 300 nm^{-1} μm; width: 100–300 nm, Figure 1B), which was also mentioned in previous studies [30, 31].

Figure 2 demonstrates further data on the characterization of MOF that was gathered by energy-dispersive X-ray analysis (EDX) and evaluated its elemental composition, which displayed the presence of carbon (54.12 wt%), nitrogen (18.51 wt%), oxygen (19.31 wt%) and iron (8.06 wt%) elements that confirms the successful synthesis of PCN-600 (Figure 2). Moreover, the elemental mapping images of the MOF approved the homogeneous scattering of all the elements (C, N, O, and Fe) throughout the structure (Figure 3).

The PXRD pattern of synthesized MOF evidently displayed the main reflection peak of $2\theta = \sim 8°$, which is related to (2 0 1) Bragg planes and is similar to that of the simulated PCN-600 (Figure 4) [32,33].

FT-IR spectrum of the fresh PCN-600(Fe) (Figure 5A) displays a wide peak centered at 3432 cm^{-1} related to –OH groups and physisorbed water molecules. The asymmetric and symmetric stretching modes of the carboxylate coordinating groups are clearly appeared at 1601 and 1407 cm^{-1}, respectively. The detected band at 1534 cm^{-1} is attributed to the imine group of the porphyrin-Fe (III) linker. FT-IR spectrum of the post-release PCN-600(Fe) displays in Figure 5B. As can be seen in Figure 5B, there is no significant change in post-release PCN-600(Fe) structure.

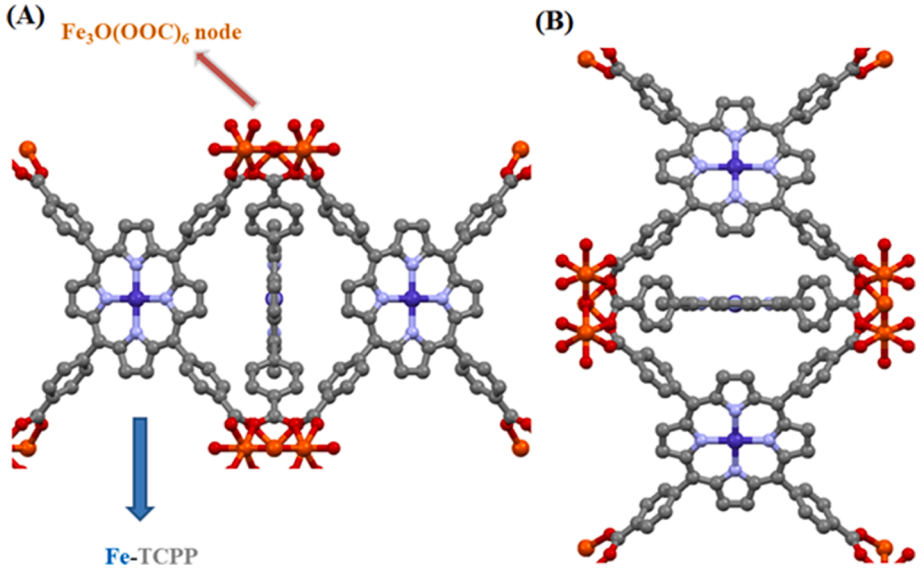

Scheme 1. Schematic representation of different views (A and B) of as-synthesized PCN-600.

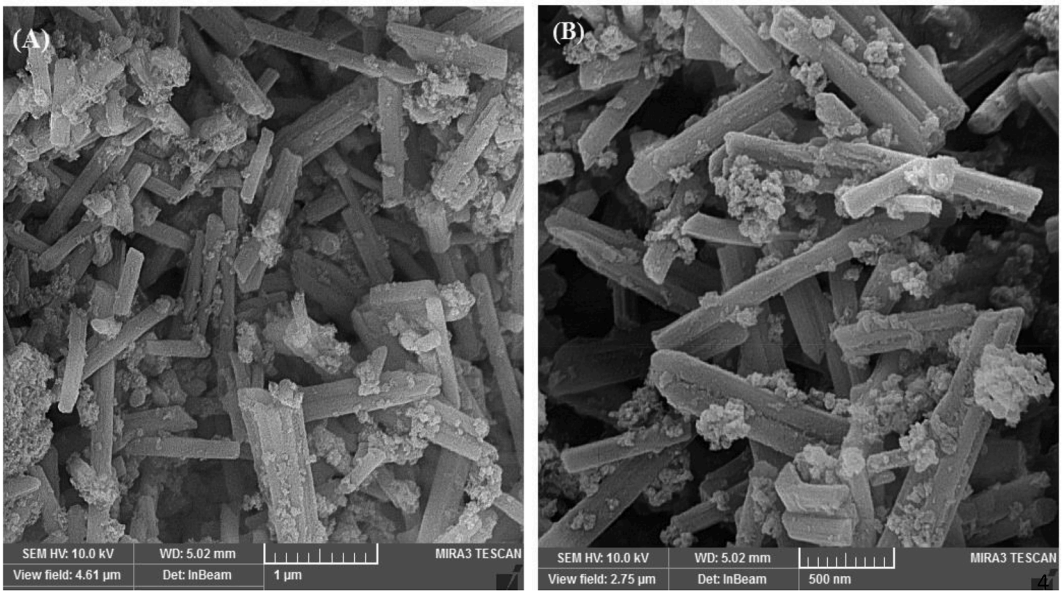

Figure 1. FESEM images of PCN-600 (A) 1 µm and (B) 500 nm magnification.

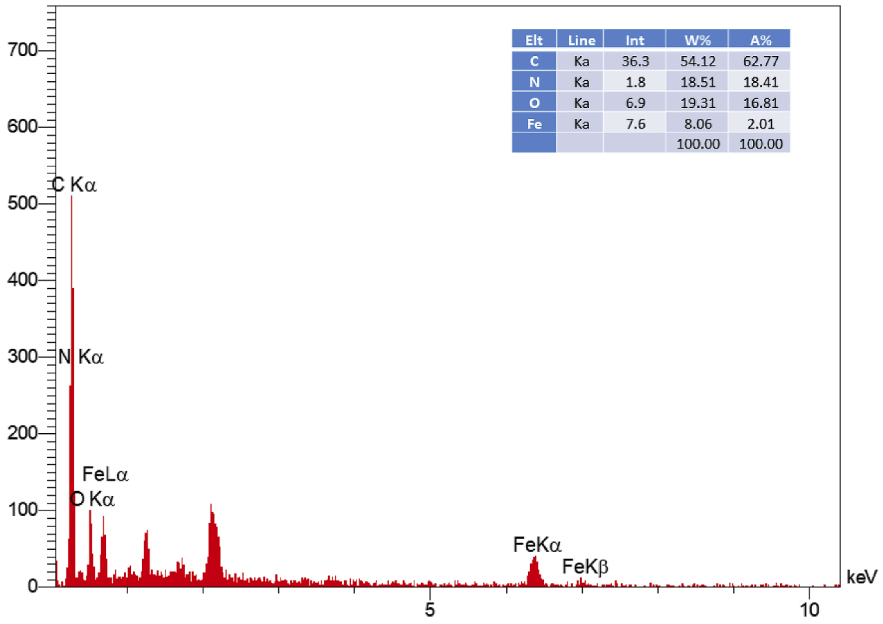

Figure 2. EDX analysis and elemental composition of PCN-600.

3.2. Loading efficiency and release study of PTX-loaded PCN-600

The parameters of the carrier and drug can influence drug loading effectiveness, which includes chemical interactions between the carrier and drug, drug solubility in the carrier, molecular weight, and volumetric size of carrier. An extended drug loading is believed to improve NP stability; however, it may also affect their pharmacodynamic and pharmacokinetic features [34, 35]. According to the results of examining the PTX loading capacity of PCN-600 in PBS at pH = 7.4, a standard curve of PTX with some concentrations was created. The loading percentage of PTX on PCN-600 was calculated to be 87.3 percent, which indicates the ability of PCN-600 in carrying an effective therapeutic payload.

We examined the UV-Vis spectrum to configure the releasing rate of PTX from PCN-600 nanoplatforms in PBS buffer at a pH of 7.4 for 48 h, which resulted in 53.5 percent of released PTX (Figure 6). The fraction of weakly entrapped PTX in PCN-600 was responsible for the first burst release. Afterwards, the PTX was released slowly and consistently, while approximately half of it remained unreleased

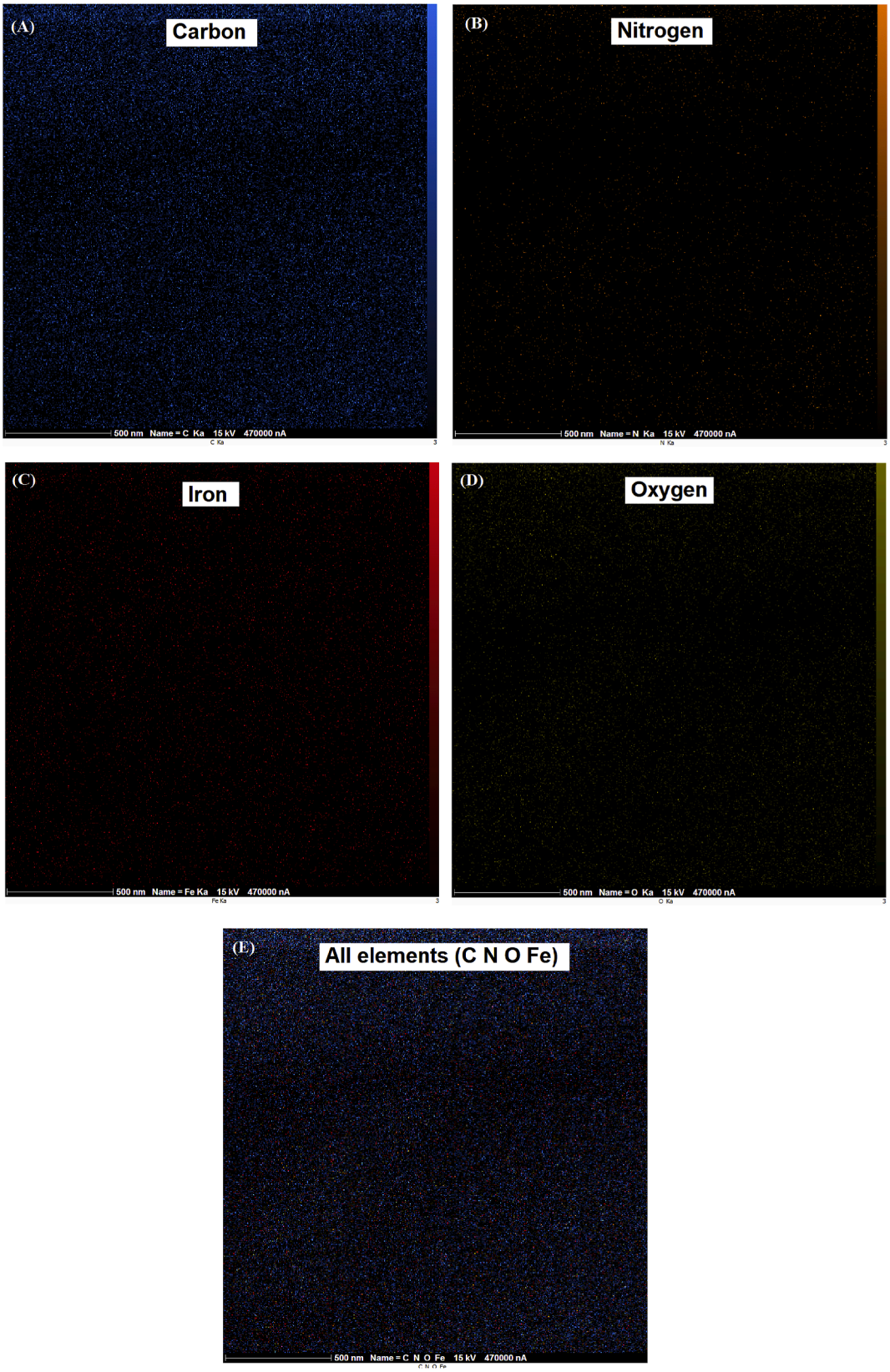

Figure 3. EDX elemental mapping images of PCN-600, (A) C element, (B) N element, (C) Fe element, (D) O element, (E) all elements.

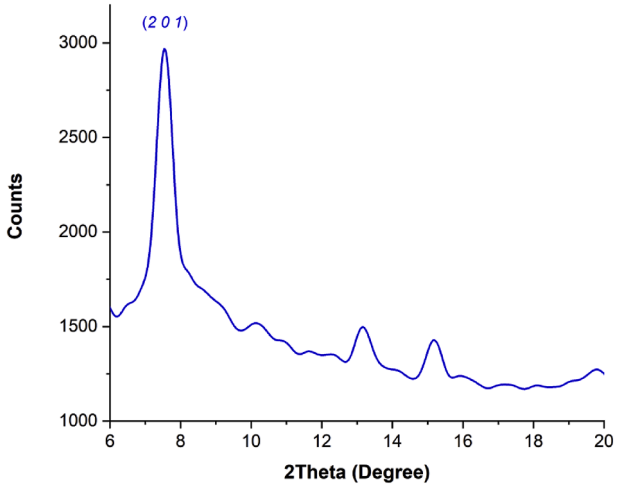

Figure 4. PXRD pattern for the PCN-600.

from the PCN-600 matrix after 48 h. Upon the application of EPR effect, such a steady and slow-release ability may suit the demands of the drug carrier, since it avoids the early release of PTX and lowers the drug toxicity before the drug carrier applies the EPR effect to passively localize the targeted tumor. These findings suggested the potential of PCN-600 in acting as an effective nanocarrier for performing efficient drug loading and regulated drug release in a malignant environment.

Many authors confirmed the promising potential of MOF NPs in functioning as a novel drug delivery system. MOF can reveal its empirical evaluation as a smart drug carrier by exhibiting a regulated releasing process throughout a specific site and an enhanced therapeutic efficacy in the absence of any supplementary exterior fields. For example, a developed PCN-221 MOF that was loaded with methotrexate (MTX) displayed a high drug loading and maintained releasing performance when subjected to a physiological environment in the lack of any "burst effects" [36]. Also, another study reported the design of a porous metal-organic construction, Zn-TBDA, that was loaded with methotrexate (MTX) through the an in-situ encapsulation, which reached a loading potential of around 12.59 wt%. In the course of diverse physiological microenvironments, MTX-encapsulated Zn-TBDA can exhibit sensitivity to pH and temperature dual-responsive releasing attitudes [37].

A summary on the outcomes of fitting the in vitro releasing data to several kinetic models is provided in Table 1. Accordingly, the remarkable agreement of the observations with Peppas kinetics distinguished and denoted the amalgamation of diffusion and erosion mechanisms as the releasing system of this set up.

3.3. Cytotoxic effect of PCN-600

We evaluated the cytotoxic activities of PTX, PCN-600, and PTX-loading PCN-600 against human breast cancer (MCF-7) cells by using an MTT assay; which the calculated IC50 value for PTX, MOF, and PTX-loading PCN-600 was 39.6 ± 0.6, 489.9 ± 1.9, and 50 ± 2.7, respectively. Compared with PTX-loading PCN-600, PCN-600 showed a lower Ic50 value, which can be a suitable carrier for delivery of PTX drug into the MCF-7 cells. According to Figure 7, the cytotoxicity of PTX drug and PTX-loading PCN-600 against MCF-7 cells was not significant at the concentration of 40 μg/mL ($p > 0.05$). Substantially higher toxicity was observed at concentrations above 40 μg/mL in the case of PTX drug than PTX-loading PCN-600, which is due to the controlled manner of PTX-loading PCN-600 in releasing drugs. As we mentioned previously, PTX-loading PCN-600 release 41.2% PTX after 24 h and 53.5 % after 48 h of incubation at pH of 7.4 (Figure 6). Therefore, PTX-loading PCN-600 requires more time to release the drug and consequently causes a lower rate of cytotoxic activity than that of PTX drug. In this regard, the IC50 value of 50 μg/mL can be considered as the optimal concentration for PTX-loading PCN-600 as an applicable data for the delivery of PTX through PCN-600.

4. Conclusion

Concisely, this work succeeded in designing and manufacturing an ideal drug delivery system, labeled as PCN-600. Foundations composed of high surface areas and satisfactory pore sizes proved to be fine candidates for PTX loading. Moreover, the unpropitious impacts of PTX induced by their release mechanisms can be minimized through the exertion of such products. Deficient cytotoxic performance, effective drug loading dimensions (around 87.3%), and a maintained distributed drug release confirms the practical value of PCN-600 as a drug carrier. In particular, the pH-responsive release of materials affirms the applicability of PCN-600 for being applied in the form of a perceptive drug carrier.

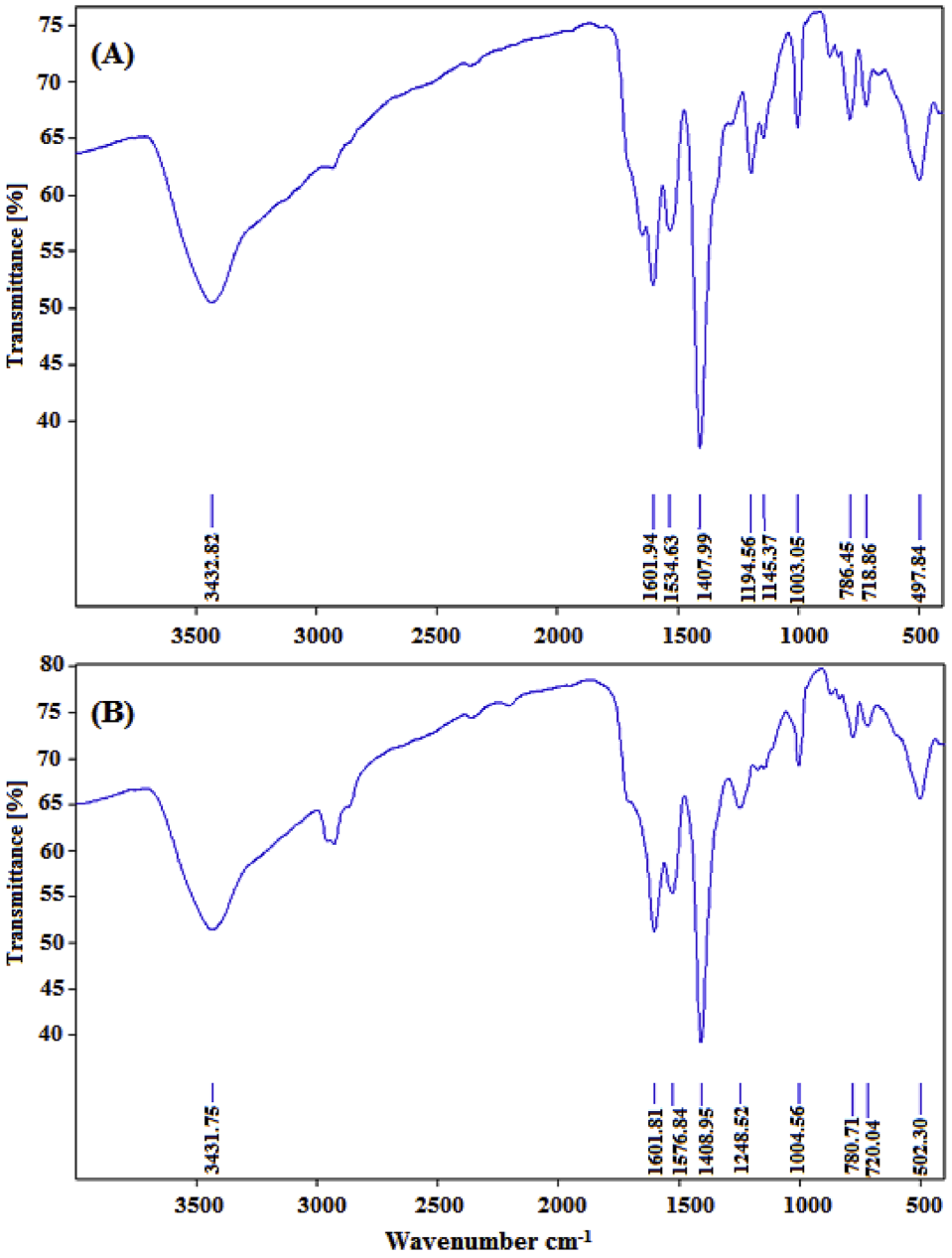

Figure 5. FT-IR spectra of the (A) as-synthesized and (B) post-release PCN-600 samples.

Declarations

Author contribution statement

Khadijeh Hamidian: Conceived and designed the experiments; Analyzed and interpreted the data; Contributed reagents, materials, analysis tools or data.

Mahmood Barani, Mina Sarani: Conceived and designed the experiments; Analyzed and interpreted the data; Wrote the paper.

Mahboubeh Adeli-Sardou: Performed the experiments.

Saba Daliran: Conceived and designed the experiments.

Ali Raza Oveisi: Conceived and designed the experiments; Performed the experiments; Contributed reagents, materials, analysis tools or data; Wrote the paper.

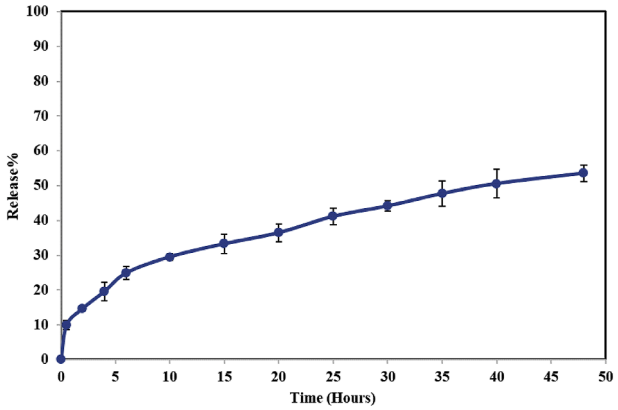

Figure 6. PTX release profile from PCN-600 under 37 °C and PBS 7.4.

Table 1
Kinetic models of PTX released from PCN-600 MOF in pH 7.4

Kinetic Model	Equation	R^2
Zero order	y = 0.0138x + 20.871	0.8268
First order	y = 0.0002x + 1.3011	0.6508
Higuchi	y = 0.9246x + 8.8343	0.9431
Peppas	y = 0.418x + 0.3407	0.9561

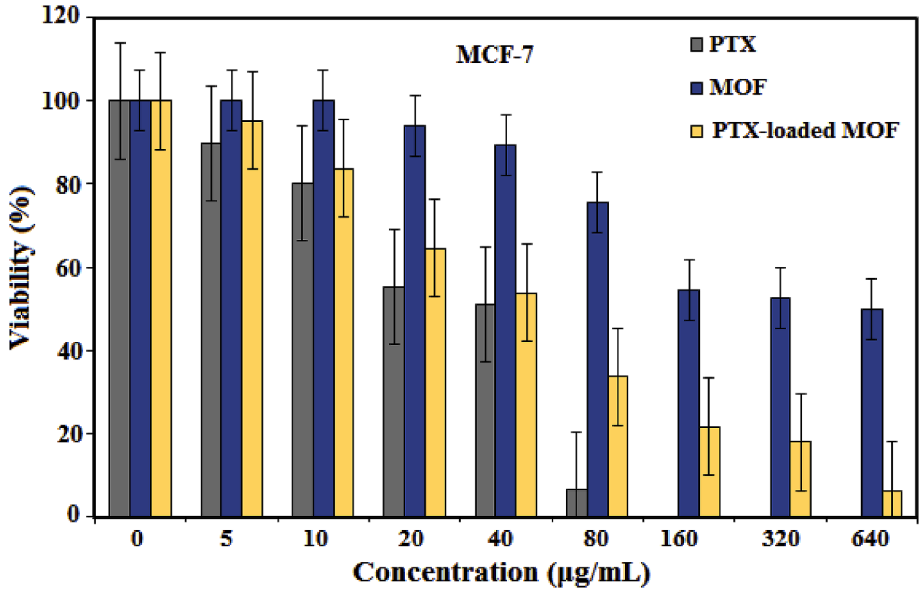

Figure 7. Cytotoxic activity of PTX, PCN-600, and PTX-loading PCN-600 against MCF-7 cells after 24 h treatment.

Funding statement

This research did not receive any specific grant from funding agencies in the public, commercial, or not-for-profit sectors.

Data availability statement

Data will be made available on request.

Declaration of interests statement

The authors declare no competing interests.

Additional information

No additional information is available for this paper.
Supplementary content related to this article has been published online at https://doi.org/10.1016/j.heliyon.2022.e12634.

References

[1] Y. Gao, Q. Shang, W. Li, W. Guo, A. Stojadinovic, C. Mannion, Y.G. Man, T. Chen, Antibiotics for cancer treatment: a double-edged sword, J. Cancer 11 (17) (2020) 5135.
[2] P. Yingchoncharoen, D.S. Kalinowski, D.R. Richardson, Lipid-based drug delivery systems in cancer therapy: what is available and what is yet to come, Pharm. Rev. 68 (3) (2016) 701–787.
[3] J.K. Patra, G. Das, L.F. Fraceto, E.V.R. Campos, M.d.P. Rodriguez-Torres, L.S. Acosta-Torres, L.A. Diaz-Torres, R. Grillo, M.K. Swamy, S. Sharma, Nano based drug delivery systems: recent developments and future prospects, J. Nanobiotechnol. 16 (1) (2018) 1–33.
[4] F. ud Din, W. Aman, I. Ullah, O.S. Qureshi, O. Mustapha, S. Shafique, A. Zeb, Effective use of nanocarriers as drug delivery systems for the treatment of selected tumors, Int. J. Nanomed. 12 (2017) 7291.
[5] F. Rossi, H. Noren, R. Jove, V. Beljanski, K.H. Grinnemo, Differences and similarities between cancer and somatic stem cells: therapeutic implications, Stem Cell Res. Ther. 11 (1) (2020) 1–16.
[6] M. Sarani, F. Tosan, S.A. Hasani, M. Barani, M. Adeli-Sardou, M. Khosravani, S. Niknam, M.A.J. Kouhbanani, N. Beheshtkhoo, Study of in vitro cytotoxic performance of biosynthesized α-Bi2O3 NPs, Mn-doped and Zn-doped Bi2O3 NPs against MCF-7 and HUVEC cell lines, J. Mater. Res. Technol. 19 (2022) 140–150.
[7] E.I. Papageorgiou, J. Subramanian, A. Karmegam, N. Papandrianos, A risk management model for familial breast cancer: a new application using Fuzzy Cognitive Map method, Comput. Methods Progr. Biomed. 122 (2) (2015) 123–135.
[8] H. Roche, L. Vahdat, Treatment of metastatic breast cancer: second line and beyond, Ann. Oncol. 22 (5) (2011) 1000–1010.
[9] J. Fares, M.Y. Fares, H.H. Khachfe, H.A. Salhab, Y. Fares, Molecular principles of metastasis: a hallmark of cancer revisited, Signal Transduct. Targeted Ther. 5 (1) (2020) 1–17.
[10] A.M. Barbuti, Z.S. Chen, Paclitaxel through the ages of anticancer therapy: exploring its role in chemoresistance and radiation therapy, Cancer 7 (4) (2015) 2360–2371.
[11] T.M. Abu Samaan, M. Samec, A. Liskova, P. Kubatka, D. Büsselberg, Paclitaxel's mechanistic and clinical effects on breast cancer, Biomolecules 9 (12) (2019) 789.
[12] N.C. Kampan, M.T. Madondo, O.M. McNally, M. Quinn, M. Plebanski, Paclitaxel and its evolving role in the management of ovarian cancer, BioMed Res. Int. 2015 (2015).
[13] S. Adepu, S. Ramakrishna, Controlled drug delivery systems: current status and future directions, Molecules 26 (19) (2021) 5905.
[14] W.F. Lai, Development of hydrogels with self-healing properties for delivery of bioactive agents, Mol. Pharm. 18 (5) (2021) 1833–1841.
[15] F. Assa, H. Jafarizadeh-Malmiri, H. Ajamein, H. Vaghari, N. Anarjan, O. Ahmadi, A. Berenjian, Chitosan magnetic nanoparticles for drug delivery systems, Crit. Rev. Biotechnol. 37 (4) (2017) 492–509.
[16] K. Hamidian, M. Sarani, E. Sheikhi, M. Khatami, Cytotoxicity evaluation of green synthesized ZnO and Ag-doped ZnO nanoparticles on brain glioblastoma cells, J. Mol. Struct. 1251 (2022), 131962.
[17] X. Xue, H. Liu, S. Wang, Y. Hu, B. Huang, M. Li, J. Gao, X. Wang, J. Su, Neutrophil-erythrocyte hybrid membrane-coated hollow copper sulfide nanoparticles for targeted and photothermal/anti-inflammatory therapy of osteoarthritis, Comp. Part. Eng. 237 (2022), 109855.
[18] C. Liu, Y. Wang, L. Li, D. He, J. Chi, Q. Li, Y. Wu, Y. Zhao, S. Zhang, L. Wang, Z. Fan, Y. Liao, Engineered extracellular vesicles and their mimetics for cancer immunotherapy, J. Contr. Release 349 (2022) 679–698.
[19] M. Chamundeeswari, J. Jeslin, M.L. Verma, Nanocarriers for drug delivery applications, Environ. Chem. Lett. 17 (2) (2019) 849–865.
[20] O.S. Fenton, K.N. Olafson, P.S. Pillai, M.J. Mitchell, R. Langer, Advances in biomaterials for drug delivery, Adv. Mater. 30 (29) (2018), 1705328.
[21] B. Baig, S.A. Halim, A. Farrukh, Y. Greish, A. Amin, Current status of nanomaterial-based treatment for hepatocellular carcinoma, Biomed. Pharmacother. 116 (2019), 108852.
[22] Q. Zeng, B. Bie, Q. Guo, Y. Yuan, Q. Han, X. Han, M. Chen, X. Zhang, Y. Yang, M. Liu, P. Liu, H. Deng, X. Zhou, Hyperpolarized Xe NMR signal advancement by metal-organic framework entrapment in aqueous solution, Proc. Nat. Acad. Sci. 117 (30) (2020) 17558–17563.
[23] F.D. Duman, R.S. Forgan, Applications of nanoscale metal–organic frameworks as imaging agents in biology and medicine, J. Mater. Chem. B 9 (16) (2021) 3423–3449.
[24] P. Trucillo, Drug carriers: classification, administration, release profiles, and industrial approach, Processes 9 (3) (2021) 470.
[25] A. Najafidoust, E.A. Asl, H.K. Hakki, M. Sarani, H. Bananifard, M. Sillanpaa, M. Etemadi, Sequential impregnation and sol-gel synthesis of Fe-ZnO over hydrophobic silica aerogel as a floating photocatalyst with highly enhanced photodecomposition of BTX compounds from water, Sol. Energy 225 (2021) 344–356.
[26] L. Feng, G.S. Day, K.-Y. Wang, S. Yuan, H.-C. Zhou, Strategies for pore engineering in zirconium metal-organic frameworks, Chem 6 (11) (2020) 2902–2923.
[27] S. He, L. Wu, X. Li, H. Sun, T. Xiong, J. Liu, C. Huang, H. Xu, H. Sun, W. Chen, Metal-organic frameworks for advanced drug delivery, Acta Pharm. Sin. B 11 (8) (2021) 2362–2395.
[28] K. Wang, D. Feng, T.F. Liu, J. Su, S. Yuan, Y.P. Chen, M. Bosch, X. Zou, H.C. Zhou, A series of highly stable mesoporous metalloporphyrin Fe-MOFs, J. Am. Chem. Soc. 136 (40) (2014) 13983–13986.
[29] Z.S. Moghaddam, M. Kaykhaii, M. Khajeh, A.R. Oveisi, Application of an iron-based porphyrinic metal–organic framework for removal of warfarin from aqueous solutions, Anal. Methods 12 (5) (2020) 651–656.
[30] S. Nazri, M. Khajeh, A.R. Oveisi, R. Luque, Enrique Rodriguez-Castellon, Mansour Ghaffari-Moghaddam, Thiol-functionalized PCN-222 MOF for fast and selective extraction of gold ions from aqueous media, Sep. Purif. Technol. 259 (2021), 118197.
[31] M. Khajeh, A.R. Oveisi, A. Barkhordar, M. Rakhshanipour, H. Sargazi-Avval, Ternary NiCuZr layered double hydroxide@ MIL-101 (Fe)-NH2 metal-organic framework for photocatalytic degradation of methylene blue, J. Nanostruct. Chem. 12 (1) (2022) 105–115.
[32] J.H. Wang, Y. Zhang, M. Li, S. Yan, D. Li, X.M. Zhang, Solvent-assisted metal metathesis: a highly efficient and versatile route towards synthetically demanding chromium metal–organic frameworks, Angew. Chem. 56 (2017) 6478–6482.
[33] K. Wang, D. Feng, T.F. Liu, J. Su, S. Yuan, Y.P. Chen, M. Bosch, X. Zou, H.C. Zhou, A series of highly stable mesoporous metalloporphyrin Fe-MOFs, J. Am. Chem. Soc. 136 (40) (2014) 13983–13986.

[34] S. Yu, X. Huang, C. Xu, L. Xu, Y. Sun, Q. Shen, B. Wang, H. Zhu, W. Lin, Q. Hu, Fabrication of metal-organic framework Mn-PBC for theranostic application, J. Solid State Chem. 313 (2022), 123349.
[35] S. Kotagudda Ranganath, M. Schlund, J. Delattre, J. Ferri, F. Chai, Bilateral double site (calvarial and mandibular) critical-size bone defect model in rabbits for evaluation of a craniofacial tissue engineering constructs, Mater. Today Biol. 14 (2022), 100267.
[36] W. Lin, Q. Hu, K. Jiang, Y. Yang, Y. Yang, Y. Cui, G. Qian, A porphyrin-based metal–organic framework as a pH-responsive drug carrier, J. Solid State Chem. 237 (2016) 307–312.
[37] W. Lin, Q. Hu, K. Jiang, Y. Cui, Y. Yang, G. Qian, A porous Zn-based metal-organic framework for pH and temperature dual-responsive controlled drug release, Microporous Mesoporous Mater. 249 (2017) 55–60.